Asociación Argentina
de Mecánica Computacional

Mecánica Computacional Vol XXXIII, págs. 429-440 (artículo completo)
Graciela Bertolino, Mariano Cantero, Mario Storti y Federico Teruel (Eds.)
San Carlos de Bariloche, 23-26 Setiembre 2014

# CAPILLARY PRESSURE SENSITIVITY IN MODELING $CO_2$ INJECTION

**Lucas A. Macias[a], Gabriela B. Savioli[b], Juan E. Santos[a], José M. Carcione[c] and Davide Gei[c]**

[a]*Laboratorio de Ingeniería de Reservorios, Instituto del Gas y del Petróleo, Facultad de Ingeniería, Universidad de Buenos Aires, Av. Las Heras 2214 Piso 3 C1127AAR Buenos Aires, Argentina, gsavioli@fi.uba.ar*

[b]*CONICET, Instituto del Gas y del Petróleo, Facultad de Ingeniería, Universidad de Buenos Aires and, Universidad de La Plata and, Department of Mathematics, Purdue University, 150 N. University Street, West Lafayette, Indiana, 47907-2067, USA, santos@math.purdue.edu*

[c]*Istituto Nazionale di Oceanografia e di Geofisica Sperimentale (OGS), Borgo Grotta Gigante 42c, 34010 Sgonico, Trieste, Italy, jcarcione@inogs.it*

**Keywords:** $CO_2$ Sequestration, Capillary Pressure, Fluid Flow Simulation

**Abstract.** Carbon dioxide ($CO_2$) sequestration consists in injecting and storage the gas into a geologic formation as a means of mitigating the greenhouse effect. Among the storage sites, saline aquifers are very promising because of their large capacity and wide availability. In this work, we perform a sensitivity analysis on the response of a flow simulator to study the impact of capillary pressure in $CO_2$ injection and storage. Capillary pressure is represented as a exponential function of $CO_2$ saturation. The simultaneous flow of $CO_2$ and brine in porous media is based on the well known Black-Oil formulation, applied to two-phase fluid flow. It considers that $CO_2$ may dissolve in the brine but the brine is not allowed to vaporize into the $CO_2$ phase. This formulation uses the PVT data as a simplified thermodynamic model. The numerical solution is obtained applying the public-domain software BOAST, which solves the differential equations by finite differences with the IMPES algorithm. Besides, we build a suitable geological model based on fractal porosity and clay content and taking into account the variation of properties with pore pressure and $CO_2$ saturation. This model also includes embedded mudstone layers of very low permeability that accumulate $CO_2$ but also allow its upward migration. Relative permeability and capillary pressure as functions of $CO_2$ saturation are taken from published data, using the Leverett $J$-function to scale capillary pressure values. The numerical results show that the fluid simulator is able to represent the $CO_2$ injection and storage. As injection proceeds, part of the injected fluid migrates upwards across the mudstone layers. The simulations are performed using different capillary pressure curves. When capillary pressure is higher, $CO_2$ upward migration is slower and, consequently, different zones of accumulations below the layers and high $CO_2$ saturations levels between layers are obtained. Thus, a precise estimation of the capillary pressure function is needed to perfom realistic long term predictions of the spatial-time $CO_2$ distribution in the underground.

## 1 INTRODUCTION

Numerical modeling of $CO_2$ injection and storage is an important tool to analyze the effectiveness of this procedure in reducing the amount of greenhouse gases in the atmosphere (Arts et al., 2008). In fact, there is no experience in the long term behavior of stored $CO_2$. The first industrial $CO_2$ injection project begins in 1996 in the Sleipner gas field in Norway. In this project, $CO_2$ separated from natural gas is being injected in the Utsira formation, a high permeable sandstone, with several mudstone layers that limit the vertical motion of the $CO_2$ (Arts et al., 2008)-(Chadwick et al., 2005).

We introduce a methodology to simulate the $CO_2$ injection and storage in saline aquifers, combined with a petrophysical model of the Utsira formation. The petrophysical model is based on initial porosity and clay content and considers the variation of properties with pore pressure and saturation (Carcione et al., 2003). Therefore, these properties are time dependent due to the $CO_2$ injection, but they change at a much slower rate than pressure and saturations. As a consequence, we have two time scales, using a much larger time step to update petrophysical properties than to run the flow simulator. The initial porosity has a fractal spatial distribution (Frankel and Clayton, 1986) and the permeability is assumed to be anisotropic and is obtained from first principles as a function of porosity and grain sizes. This geological model is able to simulate embedded mudstone layers of very low permeability.

The Black-Oil formulation for two-phase flow in porous media (Aziz and Settari, 1985) is applied to represent the $CO_2$ - brine flow. PVT data are computed from equations of state using Hassanzadeh correlations (Hassanzadeh et al., 2008). The numerical solution is obtained with the public-domain software BOAST (Fanchi, 1997), which solves the differential equations by finite differences with the IMPES algorithm (IMplicit Pressure Explicit Saturation) (Aziz and Settari, 1985). The basic idea of IMPES is to obtain a single pressure equation combining the flow equations. Once pressure is implicitly computed for the new time, saturation is updated explicitly.

Multiphase flow functions, Brine and $CO_2$ relative permeabilities and capillary pressure, are taken from published experimental data (Bachu and Bennion, 2008). The relative permeabilities are adjusted with power-law models (Savioli and Bidner, 2005), and capillay pressure is adapted to the Utsitra formation applying the Leverett $J$-function (Leverett, 1941). Besides, we test different capillary pressure curves to perform a sensitivity analysis of the simulator results.

## 2 $CO_2$ - BRINE FLOW MODEL IN POROUS MEDIA

The simultaneous flow of brine and $CO_2$ in porous media is described by the well-known Black-Oil formulation (used in petroleum simulation) applied to two-phase, two component fluid flow (Aziz and Settari, 1985). In this approach, brine is identified with oil and $CO_2$ with gas, therefore, $CO_2$ component may dissolve in the brine phase but the brine is not allowed to vaporize into the $CO_2$ phase.

The Black-Oil formulation uses, as a simplified thermodynamic model, the PVT data defined as

- $R_s$: $CO_2$ solubility in brine
- $B_g$: $CO_2$ formation volume factor
- $B_b$: brine formation volume factor

The conversion of compositional data from equations of state into the Black-Oil PVT data is performed applying an algorithm developed by Hassanzadeh et al. (2008),

- $R_s = \dfrac{\tilde{\rho}_b^{SC}\chi_g}{\tilde{\rho}_g^{SC}(1-\chi_g)}$
- $B_b = \dfrac{\rho_b^{SC}}{\rho_b(1-\omega_g)}$,

where, $\rho_b^{SC}$ and $\rho_g^{SC}$ are the brine and $CO_2$ molar densities at standard conditions and $\chi_g$ and $\omega_g$ are the $CO_2$ mole and mass fraction in the brine phase.

The differential equations, obtained by combining the mass conservation equations with Darcy's empirical law, are

$$\nabla\cdot\left(\underline{\kappa}\left(\frac{k_{rg}}{B_g\eta_g}(\nabla p_g-\rho_g g\nabla D)+\frac{R_s k_{rb}}{B_b\eta_b}(\nabla p_b-\rho_b g\nabla D)\right)\right)+\frac{q_g}{\rho_g^{SC}} = \frac{\partial\left[\phi\left(\frac{S_g}{B_g}+\frac{R_s S_b}{B_b}\right)\right]}{\partial t}, \tag{1}$$

$$\nabla\cdot\left(\underline{\kappa}\frac{k_{rb}}{B_b\eta_b}(\nabla p_b-\rho_b g\nabla D)\right)+\frac{q_b}{\rho_b^{SC}} = \frac{\partial\left[\phi\frac{S_b}{B_b}\right]}{\partial t}, \tag{2}$$

where $g$, $b$ denote gas and brine phases, respectively. The unknowns for the Black-Oil model are the fluid pressures $p_\beta$ and saturations $S_\beta$ ($\beta = b, g$). Also $\rho_\beta$ is density, $q_\beta$ injection mass rate per unit volume, $k_{r\beta}$ relative permeability and $\eta_\beta$ viscosity. Finally $\phi$ is porosity and $\underline{\kappa}$ is the absolute permeability tensor.

Two algebraic equations relating the saturations and pressures complete the system:

$$S_b + S_g = 1, \qquad p_g - p_b = P_C(S_b), \tag{3}$$

where $P_C$ is the capillary pressure.

The numerical solution was obtained employing the public domain software BOAST (Fanchi, 1997). BOAST solves the differential equations using IMPES (IMplicit Pressure Explicit Saturation), a finite difference technique (Aziz and Settari, 1985). Finite differences is the standard in commercial reservoir simulators, and the improved versions use both structured and unstructured grids with local refinements to accurately represent reservoir geometry. The basic idea of IMPES is to obtain a single pressure equation by a combination of the flow equations. Once pressure is implicitly computed for the new time, saturation is updated explicitly. We briefly describe IMPES for these particular system (1), ( 2), (3). The first step is to obtain the pressure equation, combining flow equations: Eq. (1) multiplied by $B_g$ and Eq.(2) multiplied by $(B_b - R_s B_g)$ are added. In this way, the right side of the resulting equation is:

$$B_g\frac{\partial\left[\phi\left(\frac{S_g}{B_g}+\frac{R_s S_b}{B_b}\right)\right]}{\partial t}+(B_b-R_s B_g)\frac{\partial\left[\phi\frac{S_b}{B_b}\right]}{\partial t}$$

Using the chain rule to expand the time derivatives and after some computations and rearrangements, the right side becomes:

$$\phi\left[\frac{1}{\phi}\frac{d\phi}{dp_b}+S_g\left(-\frac{1}{B_g}\frac{dB_g}{dp_b}\right)+S_b\left(-\frac{1}{B_b}\frac{dB_b}{dp_b}+\frac{B_g}{B_b}\frac{dR_s}{dp_b}\right)\right]\frac{\partial p_b}{\partial t},$$

where all time derivatives of saturation disappear.

Defining the following aproximate compressibilities,

- Formation compressibility: $c_f=\dfrac{1}{\phi}\dfrac{d\phi}{dp_b}$
- $CO_2$ compressibility: $c_g=-\dfrac{1}{B_g}\dfrac{dB_g}{dp_b}$,
- Brine compressibility: $c_b=-\dfrac{1}{B_b}\dfrac{dB_b}{dp_b}+\dfrac{B_g}{B_b}\dfrac{dR_s}{dp_b}$,
- Total compressibility: $c_t=c_f+S_gc_g+S_bc_b$,

the right side is simply expressed as,

$$\phi c_t\frac{\partial p_b}{\partial t}.$$

Finally, replacing $p_g$ by $p_b+P_C(S_b)$ in the left side of the combined equation, the following pressure equation in $p_b$ is obtained,

$$\begin{aligned}&B_g\Big[\nabla\cdot\Big(\underline{\kappa}\Big(\frac{k_{rg}}{B_g\eta_g}(\nabla p_b-\rho_g g\nabla D)+\frac{R_sk_{rb}}{B_b\eta_b}(\nabla p_b-\rho_b g\nabla D)+\frac{k_{rg}}{B_g\eta_g}\nabla P_C\Big)\Big)\Big]\\&+(B_b-R_sB_g)\Big[\nabla\cdot\Big(\underline{\kappa}\frac{k_{rb}}{B_b\eta_b}(\nabla p_b-\rho_b g\nabla D)\Big)\Big]\\&+B_g\frac{q_g}{\rho_g^{SC}}+(B_b-R_sB_g)\frac{q_b}{\rho_b^{SC}}=\phi c_t\frac{\partial p_b}{\partial t}.\end{aligned}\tag{4}$$

In BOAST simulator, system (2) , (4) is discretized using a block centered grid. The system is linearized evaluating the pressure and saturation dependent funcions (PVT parameters, viscosities, relative permeabilities and capillary pressure) in the pressure and saturation values of the previous time step. The pressure equation is solved implicitly, applying a Block Successive Over Relaxation method (BSOR) to compute the linear system solution. The saturation equation is solved explicitly, therefore stability restrictions are considered to select the time step (Savioli and Bidner, 2005).

## 3 PETROPHYSICAL MODEL OF A SHALY SANDSTONE

The pressure dependence of properties is based on the following relationship between porosity and pore pressure $p(t)=S_bp_b(t)+S_gp_g(t)$,

$$\frac{(1-\phi_c)}{K_s}(p(t)-p_H)=\phi_0-\phi(t)+\phi_c\ln\frac{\phi(t)}{\phi_0},\tag{5}$$

where $\phi_c$ is a critical porosity, $\phi_0$ is the initial porosity at hydrostatic pore pressure $p_H$ and $K_s$ is the bulk modulus of the solid grains (Carcione et al., 2003). The rock is formed with quartz (bulk modulus of 40 GPa) and clay (bulk modulus of 15 GPa). $K_s$ is computed as the arithmetic average of the Hashin Shtrikman upper and lower bounds. The relationship among horizontal permeability, porosity and clay content $C$ is (Carcione et al., 2003) ,

$$\frac{1}{\kappa_x(t)} = \frac{45(1-\phi(t))^2}{\phi(t)^3}\left(\frac{(1-C)^2}{R_q^2} + \frac{C^2}{R_c^2}\right), \tag{6}$$

where $R_q$ and $R_c$ are the average radii of the sand and clay grains. Also, as permeability is anisotropic, we assume the following relationship between horizontal and vertical permeability $\kappa_z$ (Carcione et al., 2003)

$$\frac{\kappa_x(t)}{\kappa_z(t)} = \frac{1-(1-0.3a)\sin\pi S_b}{a(1-0.5\sin\pi S_b)}, \tag{7}$$

where $a$ is the permeability-anisotropy parameter.

## 4 MULTIPHASE FLOW FUNCTIONS

Brine and $CO_2$ relative permeabilities and capillary pressure are functions of $CO_2$ saturation. We use the experimental data presented in (Bachu and Bennion, 2008). The relative permeability curves are adjusted using the following power-law models, with two parameters, the maximum value, $\kappa_r^*$, and the curvature $n$ ((Savioli and Bidner, 2005),

$$\kappa_{rg}(S_g) = \kappa_{rg}^*\Big(\frac{S_g - S_{gc}}{1-S_{gc}-S_{bc}}\Big)^{n_g} \tag{8}$$

$$\kappa_{rb}(S_g) = \kappa_{rb}^*\Big(\frac{1-S_g - S_{bc}}{1-S_{gc}-S_{bc}}\Big)^{n_b} \tag{9}$$

where $S_{gc}$ is the $CO_2$ critical saturation and $S_{bc}$ is the connate brine saturation.

We represent the relationship between capillary pressure and $CO_2$ saturation by the following exponential function,

$$P_c(S_g) = P_c^* e^{(n_c S_g)}, \tag{10}$$

where $P_c^*$ is the entry (or threshold) capillary pressure, which means the pressure at which the gas phase is sufficiently connected to allow flow.

The data presented in (Bachu and Bennion, 2008) correspond to a sandstone with different petrophysical properties than the Utsira formation. Then we apply the Leverett $J$-function (Leverett, 1941)

$$J(S_g) = \frac{P_c(S_g)}{\sigma cos\theta}\sqrt{\frac{\kappa}{\phi}} \tag{11}$$

to scale the capillary pressure curve, using porosity and permeability data of both formations. The same procedure is applied for the mudstone layers.

## 5 NUMERICAL EXAMPLES

### 5.1 Aquifer model

We consider a model of the Utsira formation having 1.2 km in the $x$-direction, 10 km in the $y$-direction and 0.4 km in the $z$-direction (top at 0.77 km and bottom at 1.17 km b.s.l.).

The simulation is performed using a mesh with equally-spaced blocks in each direction: $n_x = 300$ in the $x$-direction, $n_y = 5$ in the $y$-direction and $n_z = 400$ in the $z$-direction. Actually the model is 2.5D since the properties are uniform along the $y$-direction, which has an extension of 10 km.

The pressure-temperature conditions are $T = 31.7z + 3.4$, where $T$ is the temperature (in $^o$C) and $z$ is the depth (in km b.s.l.); $p_H = \rho_b g z$ is the hydrostatic pressure, with $\rho_b$ = 1040 kg/m$^3$ the density of brine and $g$ the gravity constant.

The initial porosity $\phi_0$ (at hydrostatic pore pressure) for the Utsira sandstone is assumed to have a fractal spatial distribution, based on the so-called von Karman self-similar correlation functions (Frankel and Clayton, 1986). Horizontal and vertical permeabilities are determined by using equations (6) and (7), considering an anisotropy parameter $a$ = 0.1 and a fixed clay content $C$ = 6 %. The spatial vertical permeability distribution at initial conditions is shown in Figure 1. It can be observed that, within the formation, there are several mudstone layers (low permebility and porosity) which act as barriers to the vertical motion of the $CO_2$.

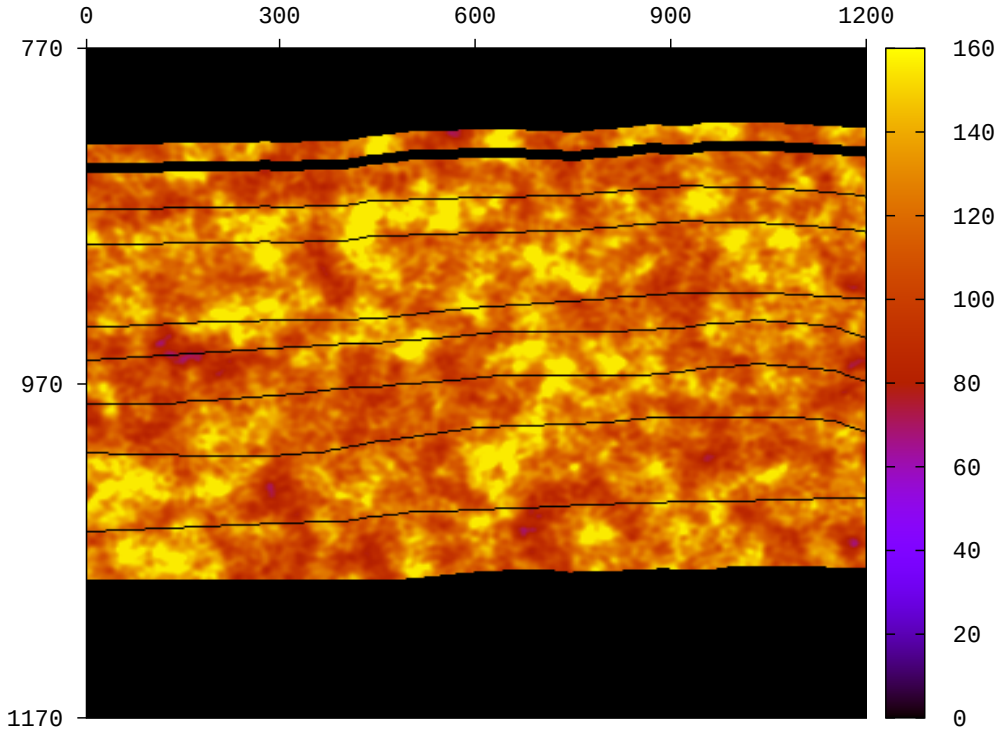


Figure 1: Vertical permeability map ($mD$)

The relative permeability curves adjusted from (Bachu and Bennion, 2008) with the power-law models (8, 9) are shown in Figure 2.

Besides, using the Leverett $J$-function we obtained the green $P_c(S_g)$ curve shown in Figure 3 for the mudstones and the red one for the Utsira formation (CASE 1).

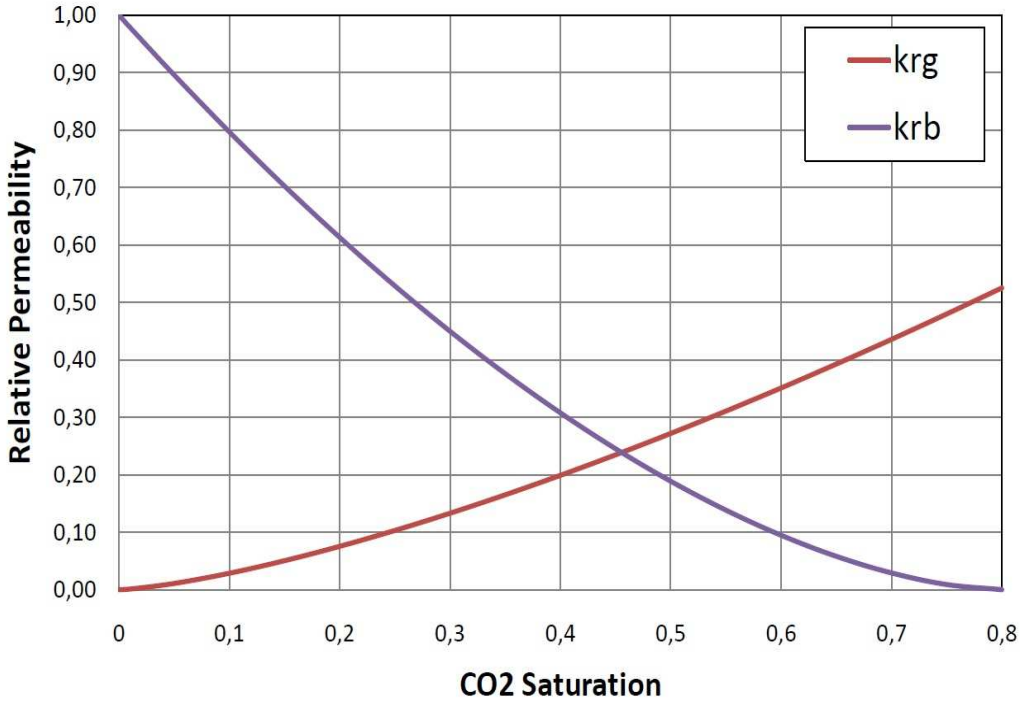


Figure 2: Relative Permeability Curves

To perform the sensitivity analysis, two other $P_c(S_g)$ curves for the Utsira formation, violet (CASE 2) and blue (CASE 3) in Figure 3, are used. They are obtained by multiplying the red curve values by 10 and 30, respectively.

### 5.2 $CO_2$ Injection

$CO_2$ is injected during three years in the Utsira formation at a constant flow rate of one million tons per year. The injection point is located at the bottom of the formation: $x$ = 0.6 km, $y$ = 5.0 km, $z$ =1.082 km. To satisfy the CFL stability condition due to IMPES formulation (Savioli and Bidner, 2005), the time step is 0.08 days. Recall that the petrophysical properties of the formation are time dependent due to the $CO_2$ injection and consequent increase in pore fluid pressure, but they change at a much slower rate than pressure and saturation. As a consequence, we have two time scales, and we use a much larger time step to update petrophysical properties than to run the flow simulator. In this work, the petrophysical properties are updated every 30 days.

Figure 4 shows the $CO_2$ saturation map after three years of injection obtained using the red (CASE 1) and green $P_c(S_g)$ curves in Figure 3 for the Utsira formation and mudstones, respectively. $CO_2$ acumulations below the mudstone layers can be observed. As $CO_2$ saturation increases, vertical permeability updated with equation 7 also increases, as it is shown in Figure 5. This allows a higher $CO_2$ mobility across the layers; therefore, part of the accumulated fluid migrates upwards, reaching the top of the formation. Porosity and horizontal permeability suffer little changes because they depend only on pressure.

Finally, we analyze the impact of capillary pressure curves on simulation results. Figures 6

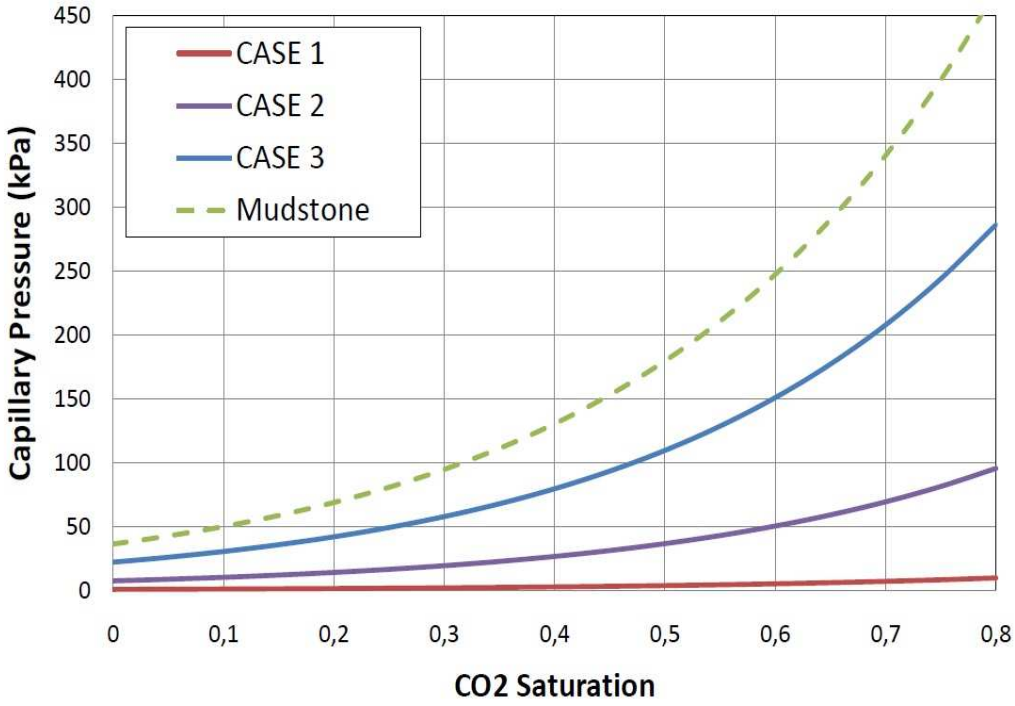


Figure 3: Capillary Pressure Curves ($kPa$)

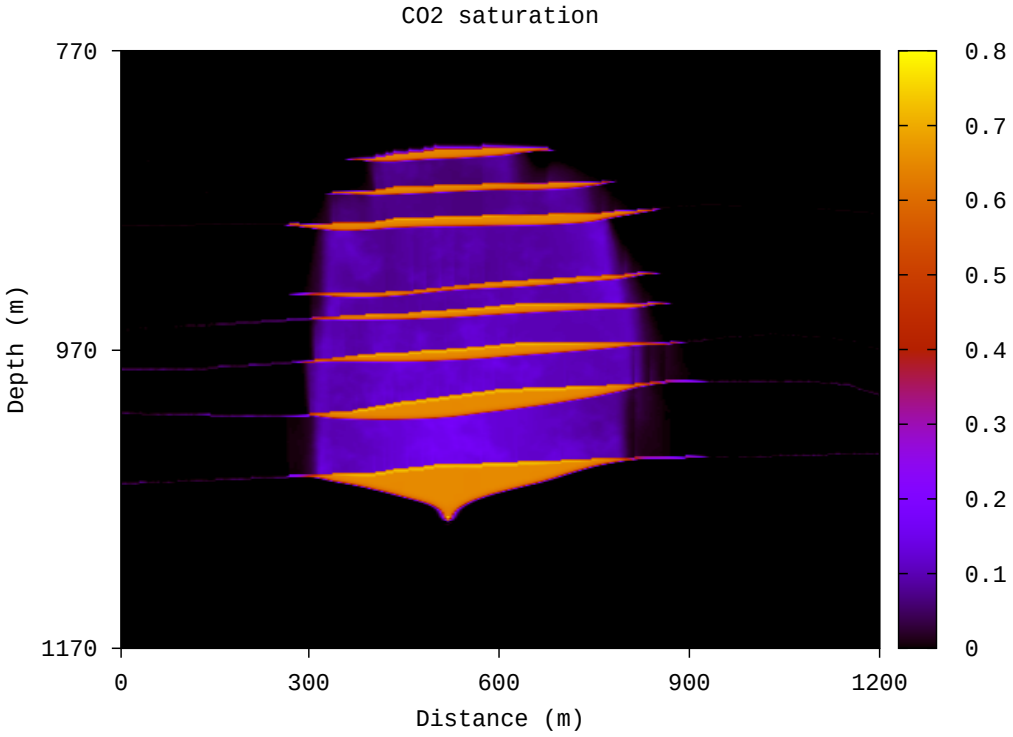


Figure 4: $CO_2$ Saturation map after 3 years of inyection: CASE 1

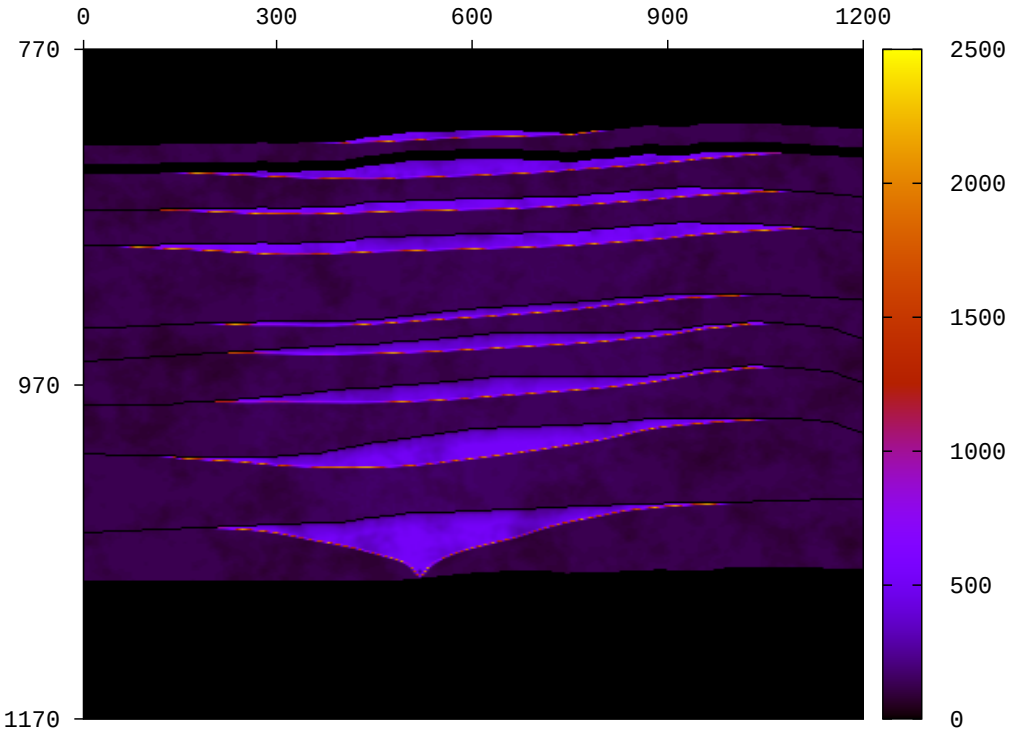


Figure 5: Vertical permeability map ($mD$) after three years: CASE 1

(CASE 2) and 7 (CASE 3) show the $CO_2$ saturation map after three years of injection obtained using the violet and blue capillary funcions shown in figure 3.

Comparing Figures 4 (CASE 1), 6 (CASE 2) and 7 (CASE 3), we can observe that the increase in capillary pressure delays the $CO_2$ upward migration. As a consequence, there are higher $CO_2$ saturations levels between layers and accumulation zones spread laterally.

In addition, higher values of vertical permeability can be observed in CASE 2 (Figure 8) and CASE 3 (Figure 9), due to the higher $CO_2$ accumulation beneath the mudsone layers. However, this vertical permeability increment that facilitates upward motion, is not enough to compensate the capillary pressure effect.

## 6 CONCLUSIONS

The fluid-flow simulator yields $CO_2$ accumulations below the mudstone layers. Capillary forces affect the migration and dispersal of the $CO_2$ plume; higher values of these forces cause a slower $CO_2$ upward migration and lateral spreading of accumulation zones below mudstone layers.

Therefore, the influence of capillary pressure is very important in $CO_2$ storage; consequently an acurate estimation of this function is essential to perfom realistic long term predictions.

Numerical simulation constitutes a meaningful tool to analyze $CO_2$ storage integrity, helping to prevent any leakage back up to the atmosphere or into underground sources of drinking water.

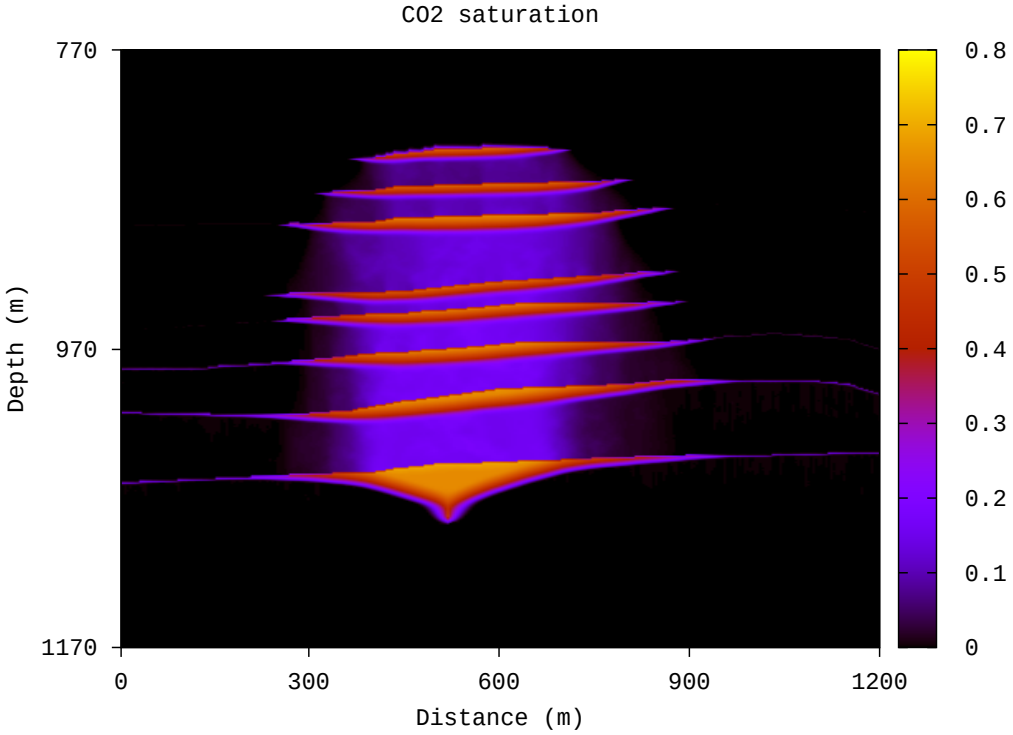


Figure 6: $CO_2$ Saturation map after 3 years of inyection: CASE 2

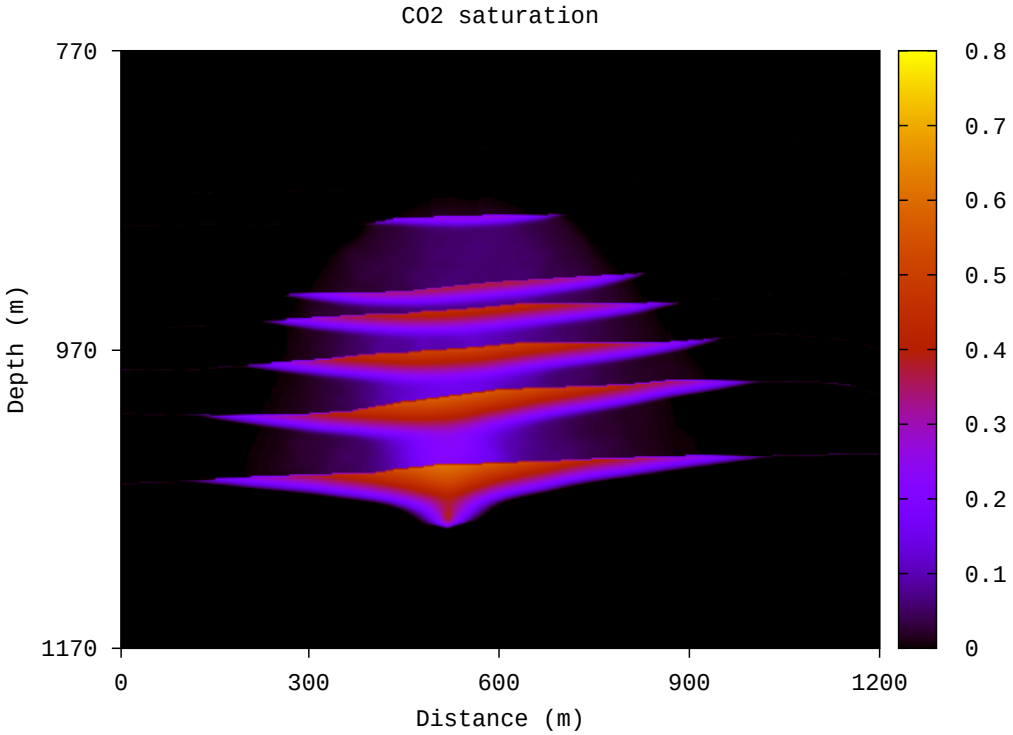


Figure 7: $CO_2$ Saturation map after 3 years of inyection: CASE 3

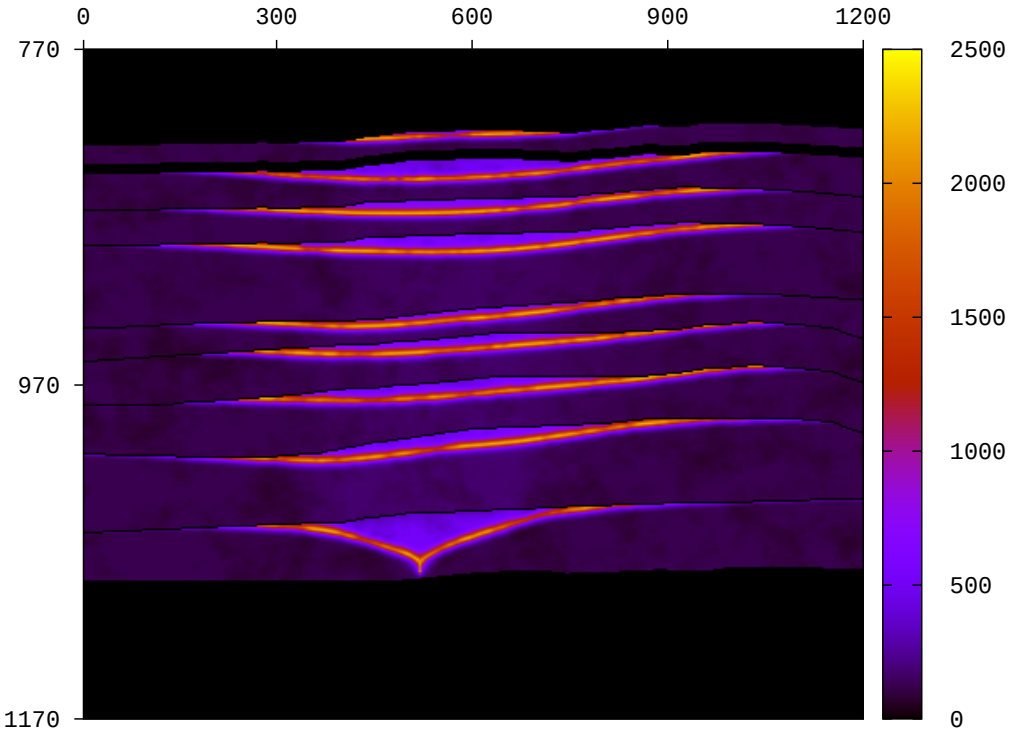


Figure 8: Vertical permeability map ($mD$) after three years: CASE 2

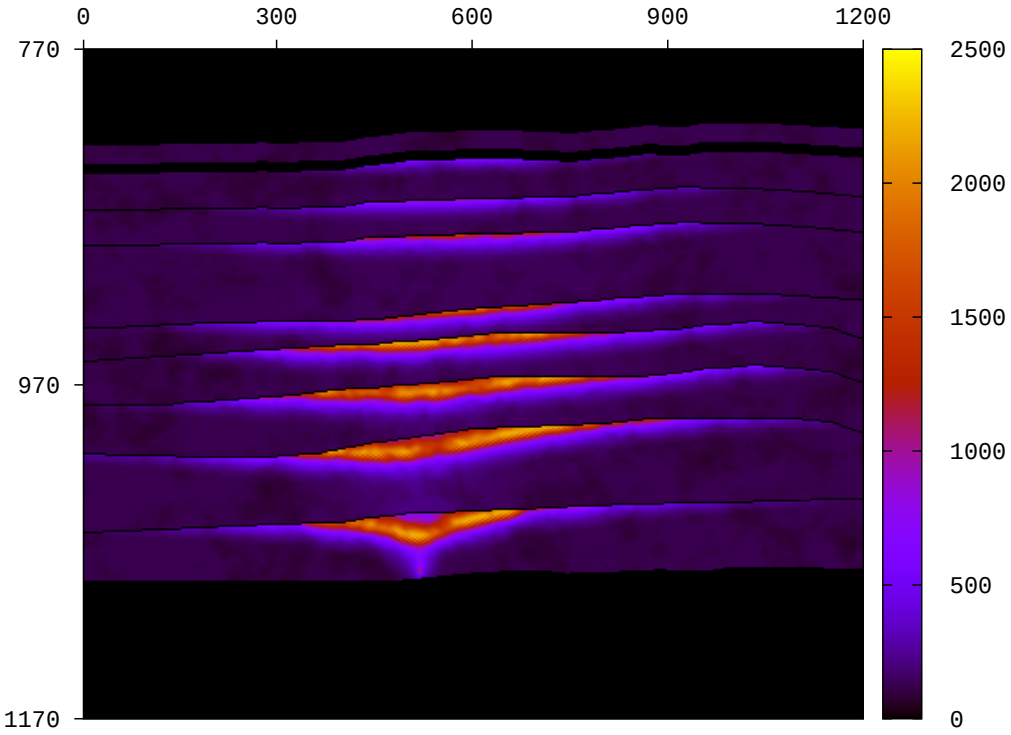


Figure 9: Vertical permeability map ($mD$) after three years: CASE 3

## 7 AKNOWLEDGEMENTS

This work was partially funded by CONICET, Argentina (PIP 0777), Universidad de Buenos Aires (UBACyT 20020120100270) and Peruilh grant provided by Facultad de Ingeniería - Universidad de Buenos Aires.

## REFERENCES

Arts R., Chadwick A., Eiken O., Thibeau S., and Nooner S. Ten years of experience of monitoring $CO_2$ injection in the utsira sand at sleipner, offshore norway. *First break*, 26:65–72, 2008.

Aziz K. and Settari A. *Petroleum Reservoir Simulation*. Elsevier Applied Science Publishers, Great Britain, 1985.

Bachu S. and Bennion B. Effects of in-situ conditions on relative permeability characteristics of $co_2$-brine systems. *Environ Geol*, 54:1707–1722, 2008.

Carcione J.M., Santos J.E., Ravazzoli C.L., and Helle H.B. Wave simulation in partially frozen porous media with fractal freezing conditions. *J. Appl. Physics*, 94:7839–7847, 2003.

Chadwick A., Arts R., and Eiken O. 4d seismic quantification of a growing $CO_2$ plume at sleipner, north sea. *Dore A G and Vincent B (Eds) Petroleum Geology: North West Europe and Global Perspectives - Proc. 6th Petroleum Geology Conference*, pages 1385–1399, 2005.

Fanchi J. *Principles of Applied Reservoir Simulation*. Gulf Professional Publishing Company, Houston, Texas, 1997.

Frankel A. and Clayton R.W. Finite difference simulation of seismic wave scattering: implications for the propagation of short period seismic waves in the crust and models of crustal heterogeneity. *Journal of Geophysical Research*, 91:6465–6489, 1986.

Hassanzadeh H., Pooladi-Darvish M., Elsharkawy A., Keith D., and Leonenko Y. Predicting PVT data for $CO_2$-brine mixtures for black-oil simulation of $CO_2$ geological storage. *International Journal of Greenhouse Gas Control*, 2:65–77, 2008.

Leverett M.C. Capillary behaviour in porous solids. *Transactions of the AIME*, 142:159–172, 1941.

Savioli G. and Bidner M.S. Simulation of the oil and gas flow toward a well - a stability analysis. *Journal of Petroleum Science and Engineering*, 48:53–69, 2005.